J. King Saud Univ., Vol. 19, *Eng. Sci*. (1), pp. 1-19, Riyadh (1427H./2006)

Effect of Ion Sizes on Separation Characteristics of Nanofiltration Membrane Systems

A. A. Hussain, M. E. E. Abashar* and I. S. Al-Mutaz

Chemical Engineering Department, College of Engineering, King Saud University, P.O. Box 800, Riyadh 11421, Saudi Arabia, E-mail address: mabashar@ksu.edu.sa

(Received 11 June 2005; accepted for publication 28 May 2006)

Abstract. The effect of the ion size on salt rejection is investigated using the Donnan steric pore model (DSPM). This model accounts for the transport phenomena occurring inside the membrane through the appropriate ion sizes. Four hydrated ions (Na^+, Mg^{2+}, Cl^-, SO_4^{2-}) are considered. The ion radius is determined from Stokes-Einstein relationship (Stokes radius), the Born's theory (Born's effective radius), and the strength of hydration (Pauling radius). Experimental data validate predictions of ion rejections. It was found that ionic hydration has strong influence on the diffusion properties of ions, which affects significantly the ion rejections. The charge density across the surface of the membrane varies according to the choice of radius of solute, causes remarkable variations in the model prediction. It was also found that the charge density should be predicted accurately to obtain the surface potential which will aid in the improvement of membrane performance and also give approximate index for fabrication of thin film composite layer membrane.

Keywords: Membrane, Mathematical modeling, Nanofiltration, Ion size.

Notation

a_i	activity of ion , mol/m^3
$C_i(0^-)$	solute feed solution concentration, mol/m^3
$C_i(\delta^+)$	solute permeate concentration, mol/m^3
$c_i(x)$	concentration of ion i within pore, mol/m^3
d	thickness of the oriented solvent layer, 0.28 mm
D_{ip}	pore diffusion coefficient of ion i, m^2/s
$D_{i\infty}$	ion bulk diffusion coefficient, m^2/s
F	Faradays constant, 96487 C mol^{-1}
j_i	flux of ion i, mol/m^2 s^{-1}

* Corresponding author.

k	Boltzmann constant,1.38066x 10^{-23} J/K
k_i	ionic partition coefficient of ion i
$K_{i,,C}$	hindrance factor for convection of ion i, dimensionless
$K_{i,d}$	hindrance factor for diffusion of ion i, dimensionless
P_{ei}	modified Peclet number of ion i, dimensionless
r_i	radius of ion i, nm
r_P	effective pore radius, nm
R_i	overall rejection of solute i, dimensionless
R	universal gas constant, 8.314 J/mol K
T	absolute temperature, K
u	solvent velocity, m/s
V_i	partial molar volume of ion, i, m^3/mol
x	axial position within the pore, m
Z_i	valence of ion i, dimensionless

Greek symbols

B_i	ion function, dimensionless
γ_i	activity coefficient of ion i within pore, dimensionless
δ	membrane thickness, m
ΔP	applied pressure, N/m^2
ΔP_e	effective pressure driving force, N/m^2
$\Delta\pi$	osmotic pressure, N/m^2
$\Delta\psi_D(0)$	Donnan Potential at the feed membrane interface,V
$\Delta\psi_D(\delta)$	Donnan Potential at the permeate membrane interface, V
ζ	ratio of effective charge density to bulk feed concentration, dimensionless
η	solvent viscosity within pores, Ns/m^2
η_o	bulk solvent viscosity, Ns/m^2
λ_i	ratio of ion radius to pore radius, dimensionless
μ_i	electrochemical potential of ion i, J/mol
ϕ_i	steric partition coefficient of ion i, dimensionless
χ	effective charge density, mol/m^3
ψ	potential within the pore, V

Introduction

There is an increased interest in focusing the use Nanofiltration (NF) membrane technology for separation processes in the chemical and biological industry because it overcomes several operational problems associated with conventional techniques. The NF membrane lies between Ultrafiltration (UF) and Reverse Osmosis (RO) with former being porous in structure and later being non-porous. NF membranes take into account the sieving and electrical effects of UF and solution diffusion of RO, which allows it to separate charged organic solutes and inorganic solutes.

The application of NF technology today includes pretreatment in sea water desalination, disinfection by the removal of virus, the removal of pesticides and other micro pollutants, arsenic removal, recovery of high value organometallic catalysts from reaction mixtures allowing the catalyst to be reused. Pharmaceutical applications include the isolation of industrially important antiviral drug precursor N-acetyl-D-neuraminic acid, clindamycin from fermentation waste water and sodium cefuroxime from cephalosporin-C [1].

In order to fully realize the application potential of NF and to properly predict the membrane performance, it is important to have a mathematical transport model. The ionic transport and the selectivity of NF membranes mainly depend on two effects: charge repulsion and steric/hydrodynamic effects. The first effect is caused by the charged nature of the membrane and electrolytes. The second effect is caused by relative size of the ions to the membrane pores. Additional phenomena can affect membrane performance namely ion-membrane affinity, specific adsorption, reduced dielectric permittivity and hydration. Models for NF are usually based either on a mechanism-independent approach, such as irreversible thermodynamics (IT) or structural mechanism dependence [2]. The models based on IT treat the membrane as a black box ignoring the structure of the membrane or any transport mechanism. Mechanistic models assume a membrane structure and the model equations account for the effects of physical and chemical characteristics of both the membrane and electrolyte solution. Most mechanistic models fall in two categories: those based on the space-charge (SC) model [3] and Teorrell-Meyer-Sievers (TMS) model [4]. The SC model is mathematically complicated and computationally expensive when compared with TMS model. Donnan steric pore model (DSPM) is an extension of TMS model with additional modifications. Original DSPM contains three fitting parameters namely, pore radius, membrane thickness and charge density. Bowen and co-workers [5] by including the partial molar volume of solute and pore viscosity resulted that NF membrane performance can be predicted by two fitting parameters namely radius of pore and charge density. The DSPM succeeded to predict the membrane performance in a limited range of operating conditions [5]. However, the semi-empirical DSPM model and other existing models suffer from many problems such as: (a) the large predicted effective charge density, (b) membrane characterization is performed through a complex fitting procedure, (c) the models fail to predict successfully the rejection of many ions. The DSPM assumes the Donnan equilibrium as the only electrostatic phenomenon involved in the ion partitioning. It is a matter of fact the Donnan equilibrium is not sufficient to explain the high rejection values of the model compared to experimental values for many ions. A physical assessment of the separation phenomena take place in many systems indicates that many factors are being taken into account implicitly in the DSPM, which result in poor quality of agreement with experimental data in many cases. To this end, general good predictive models till now do not exist for prediction of simple single salts rejections such as sodium chloride, magnesium sulphate… etc.

The objective of the present study is to implement various ion radii such as Stokes-Einstein, Born's effective and Pauling radii to develop physical realism in order to improve the agreement between DSPM model parameters and measured physical quantities. The effect of the radii on the hindrance factors was also considered. Various solutes that are considered in the present study are sodium chloride, sodium sulphate, magnesium sulphate and magnesium chloride.

Formulation of Donnan Steric Pore Model (DSPM)

The weakness of the existing models lies in the large predicted effective charge density, membrane characterization is performed through a complex fitting procedure and the models fail to predict successfully divalent ions [5]. There are, however, no existing models that consider variations of ion sizes along the membrane pores. Therefore, a one-dimensional Donnan steric pore model is developed for transport of electrolytes through nanofiltration membranes. A schematic diagram of the coordinate system used is shown in Fig. 1. The following simplifying assumptions are used in the derivation of the model equations:

1. The solution is assumed to behave ideal.
2. Transport inside the pore is due to convection, diffusion and electromigration.
3. Transport effects with convection and diffusion are corrected with hindrance factors.
4. The flow inside the pore is assumed laminar and Hagen-Poiseuille type relationship was used for solvent velocity.
5. Chemical potential of solute depends on operating pressure.
6. The solvent within the pores is consisting of one layer of oriented water molecules.
7. Variation of solvent viscosity inside the pore are considered.
8. Concentration polarization across the surface of the membrane is neglected.
9. Partial molar volume and diffusion coefficient inside pore are independent of concentration.
10. The separation inside the pore is due to steric and Donnan effect.
11. Electroviscous term is neglected for velocity of ions in the solvent.
12. The concentration and potential gradient is varied axially and radial variation is neglected.

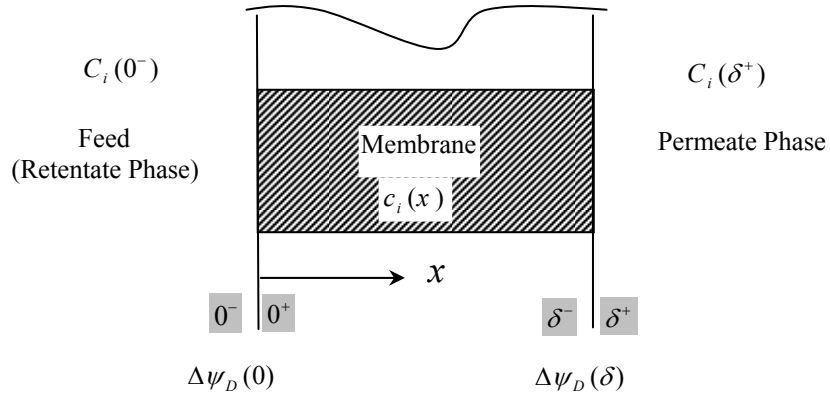

Fig. 1. Coordinate system for the DSPM.

The molar flux of ion i is given by Extended Nernst-Planck (ENP) equation as follows:

$$j_i = K_{ic} c_i u + \left(-\frac{c_i D_{ip}}{RT} \frac{d\mu_i}{dx} \right) \tag{1}$$

where K_{ic} is a hindrance factor accounting for the effects of pores walls on the species motion and is given by:

$$K_{ic} = (2-\phi_i)(1.0 + 0.054\lambda_i - 0.988\lambda_i^2 + 0.441\lambda_i^3) \tag{2}$$

and ϕ_i is the dimensionless steric partition coefficient of ion i and may be given by:

$$\phi_i = (1-\lambda_i)^2 \tag{3}$$

where λ_i is the dimensionless ratio of ion or solute radius i to pore radius and given as follows:

$$\lambda_i = \frac{r_i}{r_p} \tag{4}$$

and D_{ip} is the pore diffusion coefficient of ion i and may be given by:

$$D_{ip} = K_{id} D_{i\infty} \frac{\eta_o}{\eta} \tag{5}$$

where K_{id} is ionic hindrance factor for diffusion accounting for the effect of pore to reduce the solute-solvent diffusion coefficient below its value in the free bulk solution (water), $D_{i\infty}$ is the diffusivity of species i in water at infinite dilution. K_{id} may be written as:

$$K_{id} = 1.0 - 2.30\lambda_i + 1.154\lambda_i^2 + 0.224\lambda_i^3 \tag{6}$$

As shown in Eq. (5), the pore diffusion coefficient of ion i (D_{ip}) is affected by the change of the viscosity inside the pore (η). It has been shown by many investigators that the viscosity inside the pore increases by the decrease in pore radius [4]. The viscosity ratio is given by:

$$\frac{\eta}{\eta_o} = 1.0 + 18\left(\frac{d}{r_p}\right) - 9\left(\frac{d}{r_p}\right)^2 \tag{7}$$

where η_o is the bulk solvent viscosity.
The electrochemical potential (μ_i) is given by:

$$\mu_i = RT \ln a_i + V_i P + z_i F\psi + constant \tag{8}$$

The ion activity of species i (a_i) as a function of concentration may be given by:

$$a_i = \gamma_i c_i \tag{9}$$

Differentiating Eq. (8) and substituting in Eq. (1) yields:

$$\begin{aligned} j_i = {} & K_{i,c} c_i(x) u - D_{ip} c_i(x) \partial_x \ln \gamma_i - D_{ip} \partial_x c_i(x) - \frac{1}{RT} V_i D_{ip} c_i(x) \partial_x P \\ & - \frac{F}{RT} z_i D_{ip} c_i(x) \partial_x \psi \end{aligned} \tag{10}$$

Since the concentration inside the pore is very small, the activity coefficient term in Eq. (10) is neglected according to Debye Huckel theory [5]. Hagen-Poiseuille equation for laminar flow is used to give constant pressure gradient along the pore as follows:

$$\partial_x P = \frac{\Delta P_e}{\Delta x} = \frac{8\eta u}{r_P^2} \tag{11}$$

where ΔP_e is the effective pressure and is given by:

$$\Delta P_e = \Delta P - \Delta \pi \tag{12}$$

ΔP, $\Delta\pi$ are the applied and osmotic pressure difference across the pore respectively. Substituting Eq. (11) in Eq. (10) yields:

$$j_i = \left[K_{ic} - \left(\frac{8\eta}{RT\ r_p^2} \right) D_{ip} V_i \right] c_i\, u - D_{ip} \frac{dc_i}{dx} - \frac{F}{RT} z_i D_{ip} c_i \frac{d\psi}{dx} \tag{13}$$

Equation (13) contains three transport terms namely convection, ionic diffusion and electromigration. The molar flux (j_i) are also linked by the filtration condition:

$$j_i = C_i(\delta^+) u \tag{14}$$

Substituting Eq. (14) into Eq. (13) yields

$$\frac{dc_i}{dx} = \left[K_{ic} - \left(\frac{8\eta}{RT\ r_p^2} \right) D_{ip} V_i - C_i(\delta^+) \right] \frac{u}{D_{ip}} - \frac{F}{RT} z_i c_i \frac{d\psi}{dx} \tag{15}$$

Multiplication of Eq. (15) by z_i and summation over all ions may give:

$$\sum_{i=1}^{n} z_i \frac{dc_i}{dx} = \sum_{i=1}^{n} \left[K_{ic} - \left(\frac{8\eta}{RT\ r_p^2} \right) D_{ip} V_i - C_i(\delta^+) \right] \frac{z_i u}{D_{ip}} - \frac{F}{RT} \left(\sum_{i=1}^{n} z_i^2 c_i \right) \frac{d\psi}{dx} \tag{16}$$

The ion concentrations are bounded by electro neutrality conditions as follows:

$$\sum_{i=1}^{n} z_i C_i(0^-) = 0, \qquad \sum_{i=1}^{n} z_i C_i(\delta^+) = 0 \qquad \text{(external solution)} \tag{17}$$

$$\sum_{i=1}^{n} z_i c_i(x) = \chi_d \qquad \text{(internal solution)} \tag{18}$$

where (χ_d) is the membrane volumetric charge density.

Differentiation of Eq. (18) and substituting in Eq. (16) yields:

$$\frac{d\psi}{dx} = \frac{\sum_{i=1}^{n}\left[K_{ic} - \frac{8\eta}{RT\ r_p^2} D_{ip} V_i - C_i(\delta^+)\right]\frac{z_i u}{D_{ip}}}{\frac{F}{RT}\sum_{i=1}^{n} z_i^2 c_i} \tag{19}$$

The assumption of quasi-equilibrium at the feed and permeate-membrane interfaces allows the ionic concentration within the pore to be related to feed and permeate concentrations through partition coefficients. The ionic partition coefficient of ion i accounts for different physicochemical interactions between the ions in solution and between the ions in the pores and the membrane matrix and may be written as:

$$k_i = (steric) \times [electrostatic\ (Donnan)] \times \ldots \tag{20}$$

Equations (15) and (19) form a boundary value problem with the following boundary conditions:

$$at\ x = 0$$

$$k_i\big|_0 = \frac{c_i(x)\big|_{x=0^+}}{C_i(0^-)} = \phi_i \exp\left(-\frac{F z_i}{RT}\Delta\psi_D(0)\right),$$

$$\sum_{i=1}^{n} z_i C_i(0^-)\phi_i \exp\left(-\frac{F z_i}{RT}\Delta\psi_D(0)\right) = \chi_d \tag{21}$$

$$at\ x = \delta$$

$$k_i\big|_\delta = \frac{c_i(x)\big|_{x=\delta^-}}{C_i(\delta^+)} = \phi_i \exp\left(-\frac{F z_i}{RT}\Delta\psi_D(\delta)\right),$$

$$\sum_{i=1}^{n} z_i C_i(\delta^+)\phi_i \exp\left(-\frac{F z_i}{RT}\Delta\psi_D(\delta)\right) = \chi_d \tag{22}$$

where the Donnan potential ($\Delta\Psi_D$) for the feed and permeate side is given by:

$$\Delta\psi_D(0) = \psi(0^+) - \psi(0^-) \quad \text{(feed)}, \quad \Delta\psi_D(\delta) = \psi(\delta^-) - \psi(\delta^+) \quad \text{(permeate)} \tag{23}$$

The rejection of solute i is given by:

$$R_i = 1 - \frac{C_i(\delta^+)}{C_i(0^-)} \tag{24}$$

For uncharged solutes, dψ/dx=0 and Eq. (15) thus becomes:

$$\frac{dc_i}{dx} = \left[K_{ic} - \left(\frac{8\eta}{RT\, r_p^2} \right) D_{ip} V_i - C_i(\delta^+) \right] \frac{u}{D_{ip}} \tag{25}$$

with the following boundary conditions:

$$\begin{aligned} &at\ x = 0 \\ &k_i\big|_0 = \frac{c_i(x)\big|_{x=0^+}}{C_i(0^-)} = \phi_i \end{aligned} \tag{26}$$

$$\begin{aligned} &at\ x = \delta \\ &k_i\big|_\delta = \frac{c_i(x)\big|_{x=\delta^-}}{C_i(\delta^+)} = \phi_i \end{aligned} \tag{27}$$

Equation (25) can be integrated with the boundary conditions to give an analytical relationship for the uncharged solute rejection as follows:

$$R_i = 1 - \frac{(K_{ic} - \beta_i)\phi_i}{1 - \left[1 - (K_{ic} - \beta_i)\phi_i\right] \exp(-Pe_i)} \tag{28}$$

where β_i is dimensionless quantity given by:

$$\beta_i = \frac{8\eta}{RT\, r_p^2} D_{ip} V_i \tag{29}$$

and Pe_i is the dimensionless modified Peclet number given by:

$$P_{ei} = \frac{(K_{ic} - \beta_i) r_p^2 \Delta P_e}{8\eta D_{ip}} \tag{30}$$

Computational Procedure

Equations (15) and (19) are solved by shooting method based on Runge-Kutta Gear method and Newton-Raphson technique using FORTRAN subroutines namely DGEAR and ZSPOW. Double precision was used in all simulation.

Results and Discussion

In this study, we considered various ionic radii namely, Stokes-Einstein, Born's effective and Pauling. To familiarize the reader with these radii their definitions are given as follows:

The Stokes-Einstein radius is derived from Stokes-Einstein relation [7]:

$$r_i = \frac{k\,T}{6\pi\eta_o D_{i\infty}} \tag{31}$$

The Stokes-Einstein radius at 298.15 K is shown in Table 1 below. The dynamic viscosity of water (η_o) at 25 ^oC is taken as 0.89×10^{-3} Pa.s.

The Born's effective radius is derived from Born theory. Figure 2 illustrates the structure of solutes, which consists of bare ion radius interacting with the solvent.

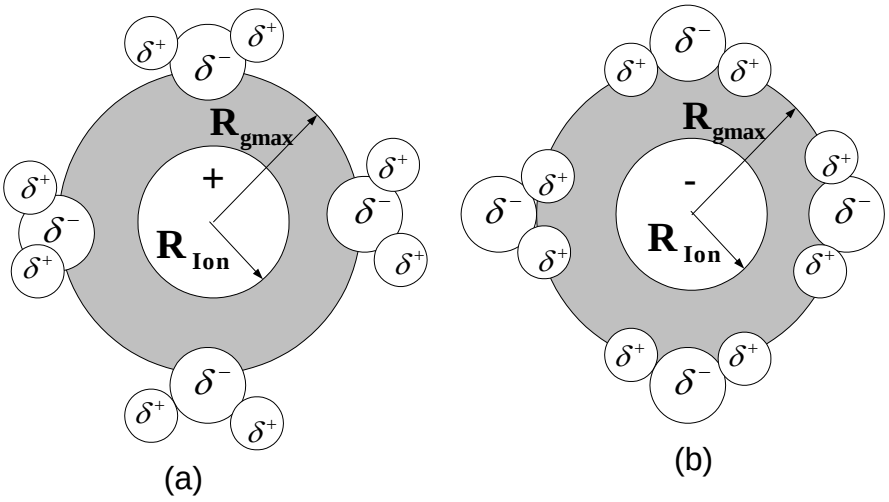

Fig. 2. A schematic diagram of the orientation of water dipoles around (a) cations and (b) anions [8].

As it can be seen that a cation is surrounded by water molecules with oxygen atoms approaching them, while an anion is surrounded by water molecules with hydrogen

atoms approaching them. R_{ion} is the ionic radius and is purely a property of the ion. R_{gmax} is defined as the position of the first peak in the ion-solvent radial distribution function; it depends on both ion and molecular nature of solvent. The Born model has been successfully used to treat the solvation free energy of an ion. However, the use of ionic radius (R_{ion}) overestimates the magnitude of the solvation energy. Babu and Lim [8] have shown by using molecular dynamics simulation of ions of varying charges, that the Born's effective radius is given by:

$$r_i = (R_{ion} + R_{g\max})/2.0 \tag{32}$$

The Born's effective radii for hydrated ions are shown in Table 1.

Pauling radius is defined as the bare ion crystal radius. Recent rejection measurements for ion mixtures using artificial nanofilters have shown that Pauling radius is the best choice [7]. The Pauling radii for hydrated ions (Na^+, Mg^{2+}, Cl^-, SO_4^{2-}) are shown in Table 1.

Table 1. Parameters used in the simulation [7-11]

	$D_{i\infty}$	V_i	r_i (nm)		
ion	**10^{-9} m^2 s^{-1}**	**cm^3 mol^{-1}**	**Stokes**	**Born**	**Pauling**
Na^+	1.33	-1.20	0.184	0.169	0.095
Cl^-	2.03	17.82	0.121	0.202	0.181
Mg^{2+}	0.72	-21.57	0.341	0.142	0.065
SO_4^{2-}	1.06	14.18	0.231	0.258	0.290

The model was validated with experimental data [5] for various feed concentrations of sodium chloride at a pressure of 0.5 MPa as shown in Table 2 using Stokes-Einstein radius. The simulations were performed by fixing the radius of pore in the membrane at r_P= 0.5 nm, which is an actual range of NF membrane. From Table 2, it was clearly shown that the model prediction in good agreement with the experimental data under these conditions.

Table 2. Comparison of experimental rejection with model rejection for sodium chloride

Concentration (M)	Experimental rejection	Model rejection
0.001	0.8214	0.8200
0.003	0.7857	0.7800
0.010	0.6800	0.6810
0.030	0.6571	0.6357
0.100	0.4285	0.4142

Figures 3, 4 and 5 show the rejection of sodium chloride versus pressure drop at different ζ for Stokes, Born and Pauling radii, respectively. The lowest rejection was observed for an uncharged membrane (ζ=0) and an increase in charge magnitude, either positive or negative resulted in an increase in salt rejection, due to relative symmetry between Na^+ and Cl^- ions in terms of charge and size.

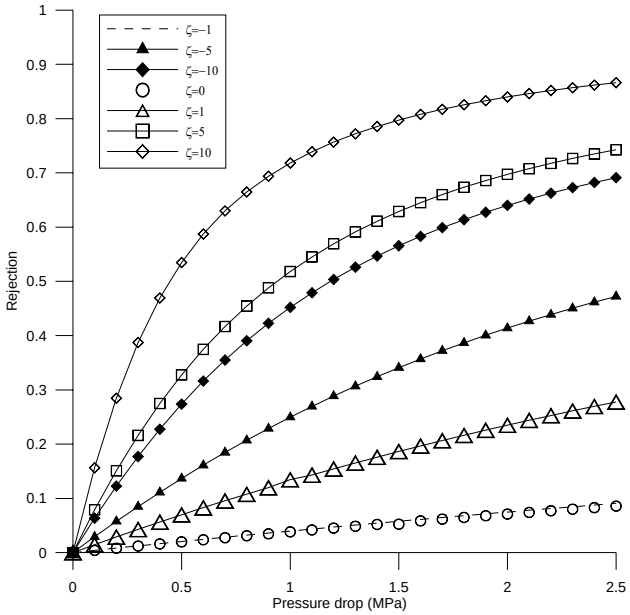

Fig. 3. Rejection of sodium chloride versus pressure drop at different ζ for Stokes-Einstein radius (r_P= 0.5 nm).

This behavior was observed for all the radii. NaCl rejection increases more with an increase in positive charge magnitude for Stokes-Einstein radius than it does with an increase in negative charge magnitude as shown in Fig. 3. When Born's effective radius was implemented as shown in Fig. 4, the magnitude of rejection for both positive and negative charges are similar with small increase in rejection for positive charge, since the size of the sodium ion is smaller than chloride. Pauling radius simulation as shown in Fig. 5 yields a different result in which the negative charge gave more rejection when compared to the positive charge. The Pauling radius of the sodium ion is smaller than chloride ion by a factor of 1.9. When using Born's effective and Pauling radii, Donnan distribution will be predominant in comparison with steric effects.

Two values of ζ (-10,10) are chosen to show the effect of ζ on negative and positive charged membrane for all radii. The results are summarized in Table 3. As it can be seen in Table 3, Born's effective radius predicted higher rejection for positive and negative charged membrane. For positively charged membrane, Stokes-Einstein

radius predicted more rejection than the Pauling radius. For negatively charged membrane, Pauling radius predicted higher rejection than the Stokes-Einstein radius. From all the results, it was inferred that the hydrated radius arise from Born theory predicted higher rejection.

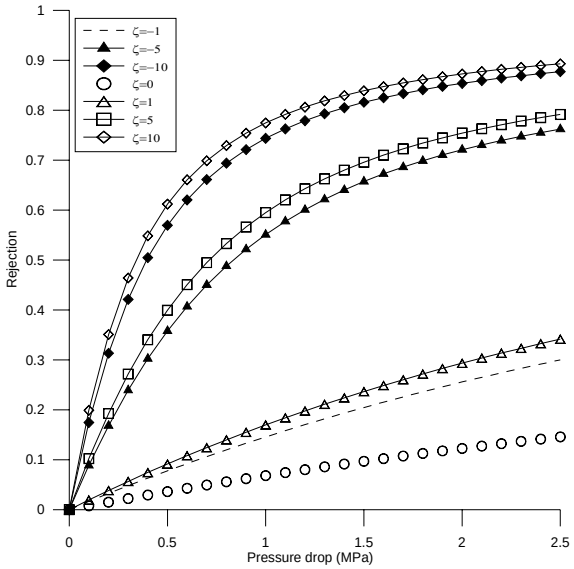

Fig. 4. Rejection of sodium chloride versus pressure drop at different ζ for Born's effective radius (r_P= 0.5 nm).

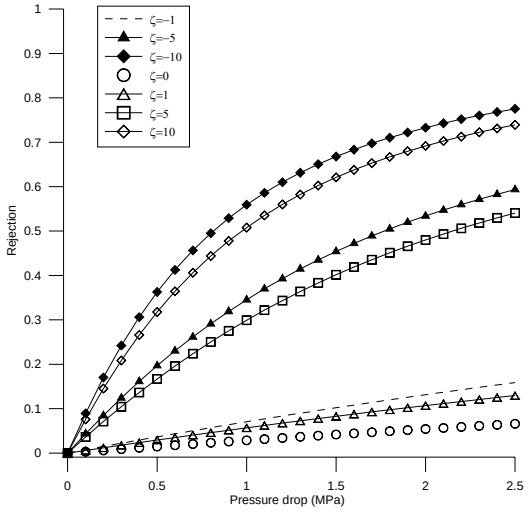

Fig. 5. Rejection of sodium chloride versus pressure drop at different ζ for Pauling radius (r_P= 0.5 nm).

Table 3. Effect of negative and positive charge density on final rejection of sodium chloride for different radii

Radius	Final rejection (%)	
	ζ=-10	**ζ=10**
Stokes-Einstein	69.11	86.61
Born	87.71	89.29
Pauling	77.53	73.91

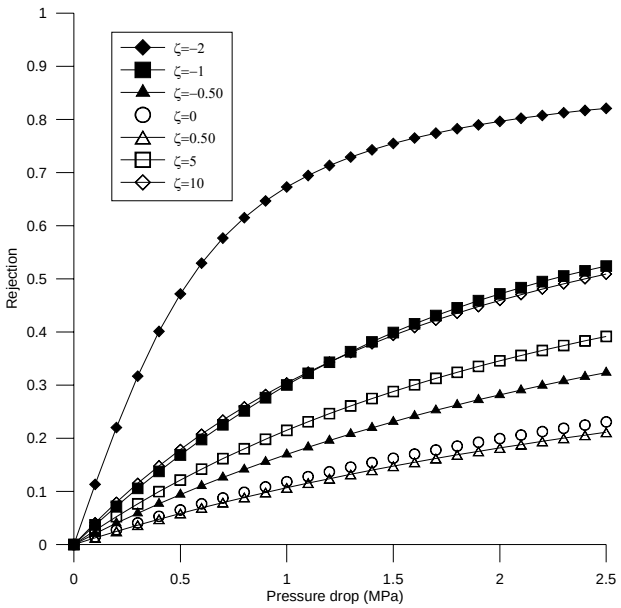

Fig. 6. Rejection of sodium sulphate versus pressure drop at different ζ for Stokes-Einstein radius (r_P= 0.5 nm).

The rejection of sodium sulphate for all the radii is shown in Figs. 6, 7 and 8. The negatively charged membrane yielded high rejection when compared to positively charged membrane for all the radii. One of the interesting features which were observed is that when the positive charge was increased, it first predicted lower rejection than uncharged membrane and after an increase in the magnitude of positive charge, there was an increase in rejection. This effect was more pronounced when Pauling radius was used.

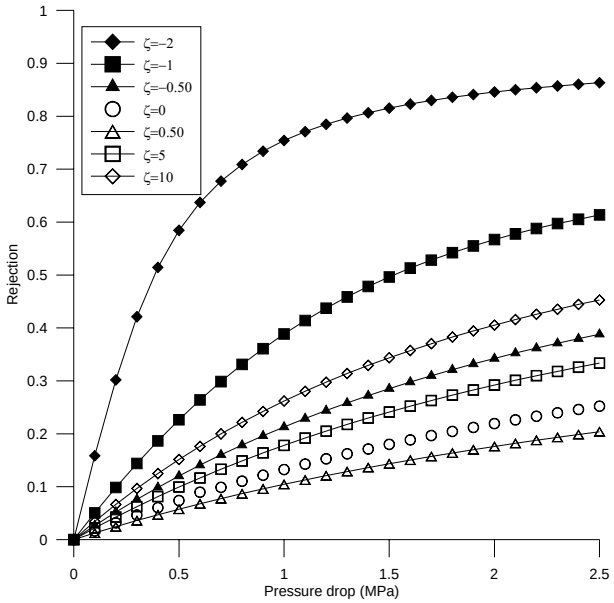

Fig. 7. Rejection of sodium sulphate versus pressure drop at different ζ for Born's effective radius (r_P= 0.5 nm).

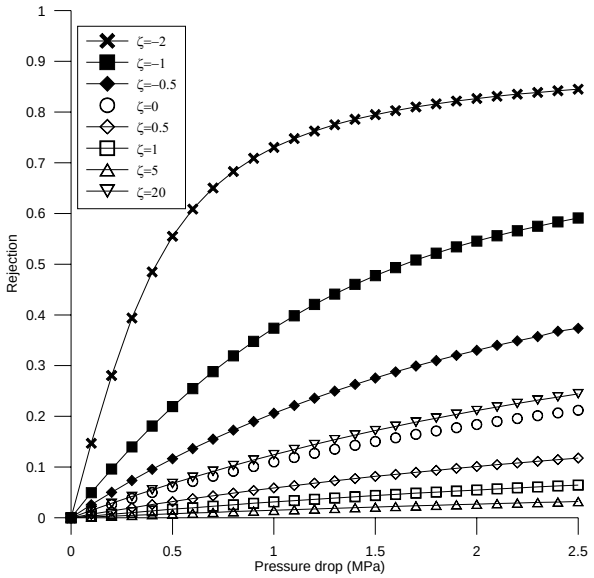

Fig. 8. Rejection of sodium sulphate versus pressure drop at different ζ for Pauling radius (r_P= 0.5 nm).

Table 4. Effect of negative and positive charge density on final rejection of sodium sulphate for different radii

Radius	Final rejection (%)	
	ζ=-2	ζ=10
Stokes-Einstein	82.09	50.88
Born	86.32	45.28
Pauling	84.50	11.66

Effect of negative and positive charge density at ζ (-2, 10) on final rejection of sodium sulphate for different radii was compared in Table 4. Stokes-Einstein radius predicted higher rejection for positively charged membrane. Born's effective radius predicted higher rejection when the membrane is negatively charged. It is evident from the analysis that the choice of the radius of the solute plays an important role in the rejection of charged solute.

Table 5 shows the final rejection for magnesium chloride for all radii at various charge densities. When the charge density (ζ) is increased, rejection was also increased. For positive charged membrane, the magnitude of rejection is high for Stokes-Einstein radius when compared to other radii.

Table 5. Final rejection of magnesium chloride for different radii

	Final rejection (%)		
ζ	**Stokes-Einstein radius**	**Born's effective radius**	**Pauling radius**
-1.0	10.55	14.50	7.95
-0.5	29.33	15.34	7.99
0.0	52.98	15.57	8.71
0.5	75.22	20.95	9.62
1.0	87.51	34.18	14.08

Table 6. Final rejection of magnesium sulphate for different radii

	Final rejection (%)		
ζ	**Stokes-Einstein radius**	**Born's effective radius**	**Pauling radius**
-1.0	63.32	39.47	45.71
-0.5	68.43	34.46	38.88
0.0	76.50	30.71	32.50
0.5	83.44	28.62	27.14
1.0	87.93	28.26	23.11

Table 6 shows the final rejection of magnesium sulphate for all radii. Stokes-Einstein radius predicted higher rejection for negative and positive charged membrane. Born radius predicted higher than the Pauling radius for positively charged membrane and it was reversed for negatively charged membranes.

Conclusions

The separation characteristics of NF membrane were studied using the Donnan steric pore model (DSPM). In addition to steric effect, the charged membrane used to have characteristics of Donnan effect. If the membrane is negatively charged, the opposite charged ions (positive ions) will be attracted by the surface of the membrane, thereby results in separation. The surface charge of the membrane is very difficult to quantify experimentally. Various radii namely Stokes-Einstein, Born's effective and Pauling were used in the DSPM. Sodium chloride, sodium sulphate, magnesium chloride and magnesium sulphate were studied as model solutes. The model was validated by sodium chloride experimental data. The minimum rejection was obtained for sodium chloride for uncharged membrane. When the charge of the membrane is increased either positive or negative resulted in increase in rejection. This phenomenon was observed for all the radii. Born's effective radius predicted higher rejection for both positive and negative charges. For sodium sulphate, Stokes-Einstein and Born's effective radii predicted higher rejection for positive and negative charged membrane. The magnitude of rejection was high for magnesium chloride when Stokes-Einstein radius was used. Born's effective and Pauling radii predicted very low rejection. For magnesium sulphate, Stokes-Einstein radius predicted higher rejection than Born's effective and Pauling radii. Born's effective radius predicted higher than the Pauling radius for positively charged membrane and it was reversed for negatively charged membranes. The present study illustrates that there is a strong interaction between the choice of the solute radii and charge density. The prediction of charge density is essential for the predictive purposes of NF membrane which give an approximate index in the fabrication of thin film composite polyamide layer. It also plays a vital role in the prediction of fouling and scaling propensity at the surface of the membrane. This work suggests that due attention should be given to ion sizes and the inclusion of dielectric exclusion and dispersion free energy to study the effect of charge density on solute radii. Further research is needed to fulfill all requirements for the wide scope of industrial applications.

References

[1] Schaefer, A.; Fane, G. F. and Waite, T. D. *Nanofiltration: Principles and Applications*. Oxford: Elsevier Advanced Technology, 2004

[2] Spiegler, K. and Kedem, O. "Thermodynamics of Hyperfiltration (Reverse Osmosis). Criteria for Efficient Membranes". *Desalination*, 1 (1966), 311-326.

[3] Gross, R. and Osterele. J. "Membrane Transport Characteristics of Ultrafine Capillaries." *J. of Chem. Phys*., 49 (1961), 228-234.

[4] Wang, X.; Tsuru, T.; Nakao, S. and Kimura, S. "Electrolyte Transport through Nanofiltration Membranes by the Space Charge Model and Comparison with Teorell-Meyer-Sievers Model." *J. of Memb. Sci.,* 103 (1995), 117-133.

[5] Bowen, W. R. and Welfoot, J. S. "Modeling the Performance of Membrane Nanofiltration: Critical Assessment and Model Development." *Chem. Eng. Sci.*, 57 (2002), 1121-1137.
[6] Bowen, W. R. and Yousef, H. N. S. "Effect of Salts on Water Viscosity in Narrow Membrane Pores." *J. of Colloid. Interface Sci.*, 264 (2003), 452-457.
[7] Lefebvre, X.; Palmeri, J. and David, P. "Nanofiltration Theory: An Analytic Approach for Single Salts." *Journal of Phy. Chem. B*, 108 (2004), 16811-16824.
[8] Babu, C. S. and Lim, C. "A New Interpretation of the Effective Born Radius from Simulation and Experiment." *Chem. Phys. Lett.*, 310 (1999), 225-228.
[9] Atkins, P. and Paula, J. D. *Atkins Physical Chemistry*. 7th ed., Oxford: Oxford University Press, 2001.
[10] Zilberbrand, M. "A Non-electrical Mechanism of Ion Exchange in Thin Water Films in Finely Dispersed Media." *Journal of Colloid. Interface Sci.,* 192 (1997), 471-474.
[11] Huheey, J. *Inorganic Chemistry: Principles of Structure and Reactivity*. 3rd ed., New York: Harper International SI Edition, 1983.

تأثير أحجام الأيون على خواص الفصل لأنظمة الترشيح بالأغشية الدقيقة جدا

إلطاف حسين ومحمد البشير أبشر وإبراهيم العناز

قسم الهندسة الكيميائية، كلية الهندسة، جامعة الملك سعود،
ص.ب. ٨٠٠، الرياض ١١٤٢١، المملكة العربية السعودية

(قدِّم للنشر في ٢٠٠٥/٠٦/١١م؛ وقبل للنشر في ٢٠٠٦/٠٥/٢٨م)

ملخص البحث. استخدم في هذه الورقة نموذج رياضي لدراسة تأثير حجم الأيون على فصل الملح، وأدخل هذا النموذج الرياضي في اعتباره ظواهر الإنتقال التي تحدث داخل الغشاء بواسطة أحجام أيونية مناسبة. استخدمت أربعة أيونات مبللة هي أيونات الصوديوم والمغنسيوم والكلور والسلفيت في هذه الدراسة. وأوجد نصف قطر الأيون بواسطة استوك انشطاين (نصف قطر استوك)، ونظرية بورن (نصف قطر بورن)، وقوة التبلل (نصف قطر باول). استخدمت النتائج المعملية لتحقيق حسابات فصل الأيون. لقد أثبتت هذه الدراسة أن تبلل الأيون له تأثير قوي على خواص الإنتشار الأيوني والتي لها تأثير قوي على فصل الأيون، وكذلك تتغير كثافة الشحنة الكهربية على سطح الغشاء بناء على اختيار نصف قطر الأيون مما يؤدي إلى اختلاف في حسابات النموذج الرياضي. وكذلك أثبتت هذه الدراسة بأن كثافة الشحنة الكهربية يجب أن تحسب بدقة للحصول على جهد سطحي يمكن أن يساعد في تحسين أداء الغشاء وإعطاء معامل تقريبية تساعد في صناعة الغشاء الطبقي الرقيق.

□